



1 Shelf Bathymetric Roughness Controls Mixing of the Persian/Arabian 2 Gulf Outflow and Arabian Sea OMZ Ventilation

3

4 Ahmed Abdelmaksoud¹, Aisha H. Al-Suwaidi¹, Gerd Bruss², Kaveh Samimi-Namin^{3,4,5},

5 Mohammed Y. Ali¹

6 ¹Earth Sciences Department, Khalifa University, 127788, Abu Dhabi, United Arab Emirates

7 ²Department of Marine Science and Fisheries, Sultan Qaboos University, Muscat, Oman

8 ³Marine Evolution and Ecology Group, Naturalis Biodiversity Center, P.O. Box 9517, 2300 RA, Leiden, The
9 Netherlands

10 ⁴Department of Biology, University of Oxford, Oxford, OX1 3SZ, UK

11 ⁵Natural History Museum, Cromwell Road, London, SW7 5BD, UK

12 *Correspondence to:* Ahmed Abdelmaksoud (ahmed.osman@ku.ac.ae; a.abdelmaksoud92@gmail.com)

13 Abstract

14 Hypersaline overflows from Marginal seas contribute to global ocean circulation and climate
15 variability. The Persian/Arabian Gulf (P/AG) contributes dense, saline, oxygenated deep outflow
16 into the Arabian Sea's Oxygen Minimum Zone (OMZ). Here, we present high-resolution
17 hydrographic mapping of the UAE-Oman margin in the northwestern Arabian Sea, integrating
18 CTD profiles, multibeam bathymetry and ROV imagery. The P/AG outflow forms a thin bottom-
19 attached layer that thickens dramatically over the rough, irregular seafloor of the unstable shelf,
20 where dilution and loss of bottom contact occur. Near-bottom salinity, oxygen, and pH decrease
21 systematically downstream in association with enhanced mixing. Distinct benthic assemblages
22 coincide with attached versus detached flow sectors, consistent with differing near-bed
23 hydrodynamic regimes. These observations indicate that bathymetric roughness controls the near-
24 field transformation of the outflow. Because outflow density depends on Gulf warming and
25 evaporation, modest climatic shifts may alter detachment depth, pathway geometry, and
26 intermediate-depth ventilation of the Arabian Sea OMZ.

27 Short Summary

28 The Persian/Arabian Gulf exports a dense, salty, oxygen-rich current that helps ventilate the
29 Arabian Sea. Measurements along the northern margin of the Gulf of Oman show that the flow
30 remains thin and attached over smooth seafloor, but thickens, mixes, and detaches over the rough



31 terrain of the shelf. These changes affect oxygen delivery and benthic life, and also suggest that
32 climate-driven density shifts may alter their pathways and impacts.

33 **1 Introduction**

34 Marginal seas produce water masses with properties distinct from the open ocean and provide
35 pathways for climate signals to penetrate the ocean interior (Melet et al., 2022). Net evaporation
36 in basins such as the Persian/Arabian Gulf (P/AG), the Mediterranean, and the Red Sea increases
37 salinity and drives dense outflows into adjacent basins. Exchange between marginal seas and the
38 open ocean is often regulated by hydraulic controls, and the resulting overflows undergo strong
39 diapycnal mixing due to bottom friction, turbulence, and entrainment, substantially modifying
40 their properties (Melet et al., 2022; Peters and Johns, 2005; Pratt and Lundberg, 1991).

41 This study focuses on the Oman–UAE margin of the northeastern Arabian Plate, where the P/AG
42 outflow enters the Gulf of Oman as the northwestern mouth of the Arabian Sea and interacts with
43 a broad continental shelf characterized by strong spatial variability in seafloor morphology. P/AG
44 water is characterized by high salinity, temperature, and comparatively elevated oxygen content
45 (Brewer and Dyrssen, 1985; Yao and Johns, 2010; Swift and Bower, 2003; Font et al., 2024). It
46 exits the Gulf as a dense near-bottom flow through the Strait of Hormuz, entraining ambient water
47 until reaching neutral buoyancy at relatively shallow intermediate depths. The outflow then
48 follows the southern margin of the Gulf of Oman as a gravity-driven current and spreads into the
49 Arabian Sea and the broader Indian Ocean, with its signature traceable as far as the Bay of Bengal
50 (Bower et al., 2000; Jain et al., 2017; Sheehan et al., 2020; Ezam et al., 2010; Prasad et al., 2001).

51 Dynamical processes within the Gulf of Oman, such as eddy–topography interactions and
52 mesoscale eddy field strain, play a central role in determining the open-ocean signature of P/AG
53 water (L'hégaret et al., 2015; Queste et al., 2018; Vic et al., 2015; L'hégaret et al., 2016; Font et
54 al., 2024). Such eddies can trap and redistribute the outflow, while double-diffusive processes such
55 as salt fingering have been observed beneath the plume in the Arabian Sea (Turner, 1967;
56 L'Hégaret et al., 2021).

57 The Arabian Sea Oxygen Minimum Zone (OMZ) ranks among the strongest globally, with suboxia
58 spanning much of the intermediate depths in its northern and northeastern sectors, including the



59 Gulf of Oman (Rixen et al., 2020; Schmidt et al., 2021). OMZs host distinctive biogeochemical
60 pathways and exert a significant influence on carbon and nitrogen cycling relative to their area,
61 shaping ecosystems through habitat compression and contributing to outgassing of greenhouse
62 gases (Gruber and Galloway, 2008; Hood et al., 2023; Stramma et al., 2010). Nearby source waters,
63 notably P/AG water, are estimated to oxygenate ~35% of the OMZ (Davila et al., 2023).
64 Consequently, it is poised to respond rapidly to variations in P/AG water properties (Ditkovsky et
65 al., 2023; Hood et al., 2023; Lachkar, 2019; Lachkar et al., 2023; Lachkar et al., 2022).

66 Despite decades of study, key aspects of the near-field transformation of P/AG water remain poorly
67 constrained, including outflow thickness variability, detachment behaviour, bathymetric controls
68 on mixing, downstream oxygen modification, and links between physical structure and benthic
69 communities. Here we present high-resolution observational mapping of the P/AG outflow along
70 the Oman–UAE margin using CTD profiles, multibeam bathymetry, and ROV imagery. The
71 dataset resolves spatial variability in outflow thickness, identifies zones of bottom attachment and
72 detachment, documents downstream oxygen and pH modification, and reveals benthic
73 assemblages consistent with boundary-layer structure.

74 **2 Data and Methods**

75 **2.1 Data**

76 This study uses 50 Conductivity–Temperature–Depth (CTD) profiles collected in the Gulf of
77 Oman, offshore Fujairah, between 9 and 18 July 2025 (Fig. 1). Profiles were obtained using a Sea-
78 Bird SBE 19plus V2 SeaCAT CTD (4 Hz). Data were quality-controlled, and only downcast
79 measurements were used because upcast measurements were affected by winch motion. High-
80 resolution multibeam bathymetry was collected using a Kongsberg EM712 system with Seafloor
81 Information System (SIS) software. This bathymetry dataset can be accessed from Abdelmaksoud
82 et al. (2025a).

83 **2.2 Methods**

84 CTD data were processed and visualized using Ocean Data Viewer (ODV; Schlitzer, 2024) and
85 the TEOS-10 GSW MATLAB toolbox (Mcdougall and Barker, 2011). Vertical sections were
86 generated for salinity, temperature, dissolved oxygen, pH, and turbidity. The P/AG water fraction



87 (P/AG_{wf}) was calculated following Font et al. (2024) based on the composite-tracer approach of
 88 Jenkins (1999). The endpoints used are 1°C and 34.86 g/kg for IODW, 29.56°C and 41.04 g/kg
 89 for P/AG water, and 23.45°C and 36.37 g/kg for IOCW, similar to those of Font et al. (2024).

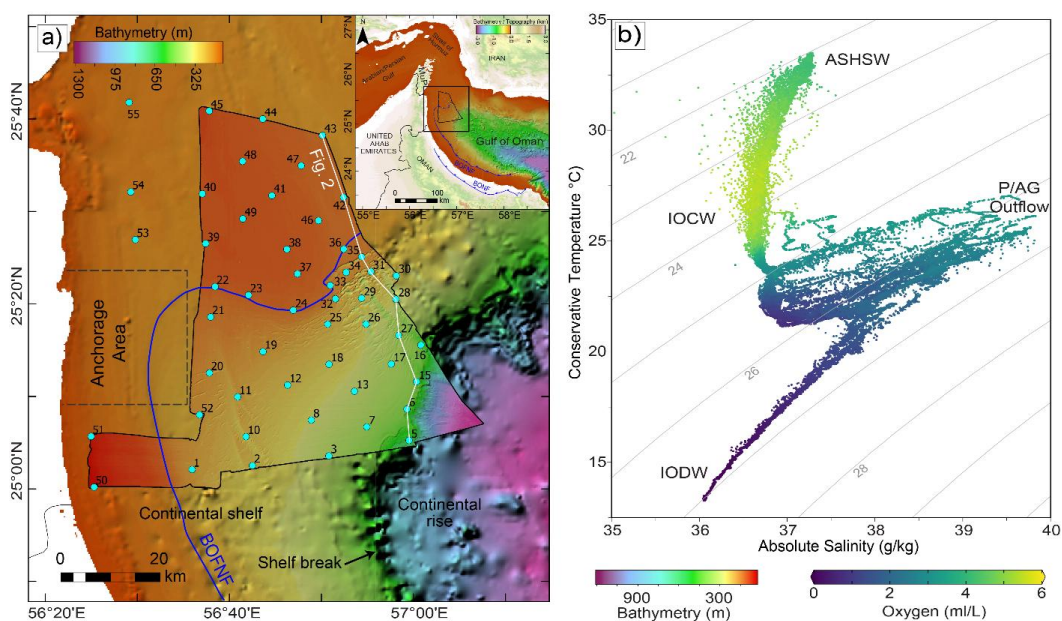


Figure 1. Bathymetry and CTD data. a) A high-resolution multibeam bathymetry of the northwestern Arabian Sea superimposed over regional bathymetry, showing acquired CTD data, with an inset showing the P/AG and the Gulf of Oman as the mouth of the Arabian Sea. b) Absolute salinity versus conservative temperature plot showing four distinct water masses across the water column of the Arabian Sea. BOFNF stands for Batinah Offshore Normal Fault; ASHSW, Arabian Sea High Salinity Water; IOCW, Indian Ocean Central Water; IODW, Indian Ocean Deep Water; P/AG Outflow, Persian/Arabian Gulf Outflow.

90 Parameter maps were produced for the deepest measurements (~5 m above the seafloor).
 91 Additional maps of plume top, bottom, and thickness were derived using a P/AG_{wf} threshold of
 92 ≥ 0.3 . This threshold represents water parcels in which P/AG contributes at least 30% of the local
 93 mixture and remains a substantial hydrographic component of the outflow. This more conservative
 94 threshold excludes weak peripheral P/AG water influence and better isolates the dynamically
 95 coherent mixed plume. Whereas core is defined by P/AG_{wf} ≥ 0.55 , corresponding to mixtures in
 96 which P/AG water is the dominant water mass component. Turner angle (Tu) and Brunt-Väisälä
 97 frequency (N^2) were calculated. ROV imagery was used to assess relationships between benthic



98 communities and the outflow, and multibeam bathymetry was analyzed to evaluate topographic
99 controls on plume structure.

100 **3 Results**

101 **3.1 Water column stratification in the Gulf of Oman**

102 Four distinct water masses were identified at the mouth of the Gulf of Oman during summer (Fig.
103 1b). The upper layer, termed Arabian Sea High-Salinity Water (ASHSW), is shallow and
104 characterized by an absolute salinity of ~ 37.2 g kg⁻¹ and temperature of ~ 33 °C. Indian Ocean
105 Central Water (IOCW) has a salinity of ~ 36.6 g kg⁻¹ and temperature of ~ 28 °C. The P/AG outflow
106 exhibits very high salinity (37.0–39.8 g kg⁻¹) and moderate temperatures of 20–27 °C. Indian
107 Ocean Deep Water (IODW), the deepest layer, has lower temperatures (~ 13 –20 °C) and salinities
108 (~ 36.0 –37.0 g kg⁻¹). Oxygen concentrations are 4–5 ml L⁻¹ in the Arabian Sea High-Salinity Water
109 and 5–6 ml L⁻¹ in IOCW. The P/AG outflow shows intermediate values (1.5–3.5 ml L⁻¹), whereas
110 IODW exhibits the lowest oxygen (< 1 ml L⁻¹).

111 **3.2 Characteristics and thickness variability of the P/AG outflow**

112 The outflow forms a distinct layer characterized by elevated salinity, temperature, oxygen, and pH
113 (Fig. 2a,b). As the outflow enters the Gulf of Oman, it separates into three lateral sectors. Across
114 the mouth of the Gulf of Oman over relatively flat bathymetry, properties are highest (salinity
115 ~ 39.0 g kg⁻¹, temperature ~ 26 °C, oxygen ~ 3.0 ml L⁻¹, pH ~ 8.51 ; Figs. 2a,c,e; 3a–c). Over the
116 shelf of the Arabian Plate, characterized by pockmarks and erosional features, values decrease to
117 ~ 38.5 g kg⁻¹, ~ 23.5 °C, ~ 2.5 ml L⁻¹, and pH ~ 8.42 . Farther south over the lower shelf and upper
118 slope, properties decline further (~ 37.2 g kg⁻¹, ~ 22 °C, ~ 2.0 ml L⁻¹, pH ~ 8.35). The western extent
119 of the outflow corresponds to bathymetric constraints, with the shallowest occurrence at ~ 110 m
120 depth. A high-turbidity layer occurs above the seafloor and thickens basinward from ~ 20 m above
121 the flat shelf to > 400 m above the upper slope (Fig. 2a,b). P/AG_{wf} values reach ~ 0.7 over the stable
122 shelf and exhibit along-flow lateral variations, largely coincident with the rough, eroded
123 bathymetry. The outflow core and plume are thin over the stable shelf and are disrupted by rough
124 bathymetry (Fig. 2i). The core fades shortly after these flow disruptions. The ratio between
125 roughness height and plume thickness (hr/H) is used as a measure of the dynamical interaction



126 between the P/AG outflow plume and the seabed (Fig. 2j). The top of the outflow occurs at depths
127 of 50–100 m above the flat shelf, with a very thin layer that has a thickness of 10–30 m, exhibiting
128 a southeastward deepening and thickness increase (Fig. 3e-f). The upper depth of the P/AG outflow
129 increases up to 170 m in the center, then becomes shallower at the extreme southern portions,
130 reaching ~130–140 m (Fig. 3e). The thickness increases up to 200 m above the lower shelf and
131 upper slope (Fig. 3f).

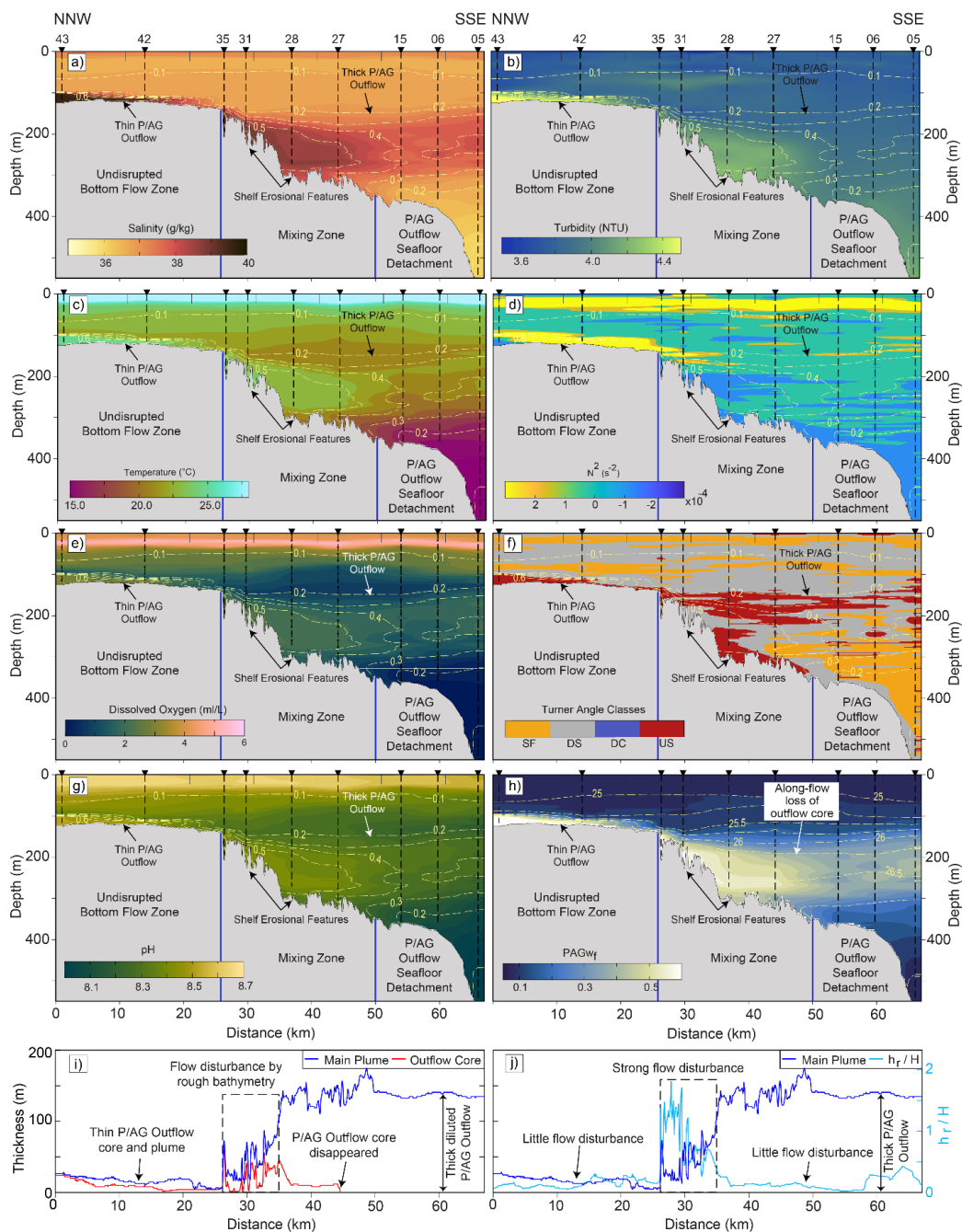


Figure 2: An NNE-SSW CTD transect (along P/AG outflow path) showing P/AG outflow and its relation to the seafloor irregularities. The parameters include salinity (a), turbidity (b), temperature (c), Brunt-Väisälä frequency (d), dissolved oxygen (e), Turner angle (f), pH (g), and P/AGW_f (h). i) Along-transect thickness of the P/AG outflow



core and main plume. j) The local seabed roughness relative to the height and plume thickness (hr/H), plotted with the plume thickness. a-g are superimposed by P/AGw_f contours, whereas h is superimposed by density contours. SF stands for salt fingering; DS, doubly stable; DC, diffusive convection; US, unstable.

132 3.3 Benthic evidence for P/AG outflow bottom attachment-detachment

133 Near-seafloor parameters (Fig. 3a–c) show sharp lateral transitions (salinity 38–36 g kg⁻¹,
134 conservative temperature 25–15 °C, oxygen 3 to <0.5 ml L⁻¹) across the depth range where the
135 outflow shifts from bottom-attached to detached flow. Where the outflow remains attached (Fig.
136 4c), the seabed consists of exposed or semi-consolidated substrate with little fine-sediment drape,
137 consistent with persistent near-bottom shear and resuspension. At deeper sites where the near-
138 bottom hydrographic signature of the outflow weakens (Fig. 4d), the seafloor is dominated by fine-
139 sediment accumulation beneath a detached outflow layer.

140 ROV imagery from ~284 m depth (Fig. 4c) shows a conspicuous epibenthic community on hard
141 or firm ground, dominated by sessile suspension feeders. Branching azooxanthellate scleractinian
142 colonies and octocorals are common, with additional scattered epifauna on exposed patches of
143 substrate. This assemblage is consistent with a relatively energetic bottom boundary layer
144 associated with the attached outflow. **By contrast**, imagery from ~360 m depth (Fig. 4d) shows a
145 flat, soft-sediment seabed with sparse epifauna; tube anemones, consistent with cerianthids, are
146 present and locally abundant. This shift, from coral-bearing hard-substrate assemblages to soft-
147 sediment, cerianthid-dominated assemblages, coincides with the hydrographic transition,
148 providing an independent benthic indicator of attachment and separation of the outflow along the
149 margin.

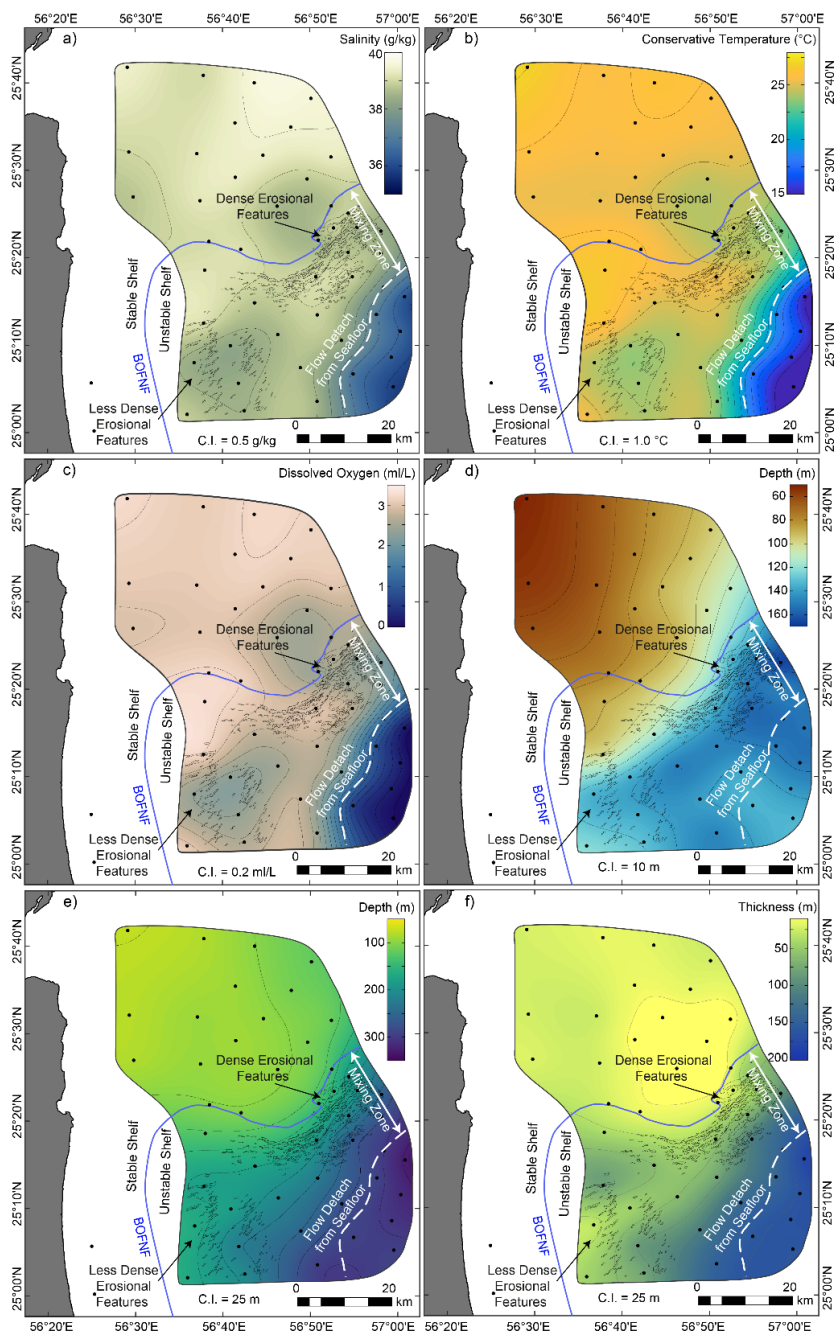


Figure 3: Near-seafloor parameters maps, as well as maps for outflow top depth, bottom and thickness. CTD maps above the seafloor, including salinity, conservative temperature, and oxygen content (a, b, c, respectively). The top, bottom, and thickness variation of the P/AG outflow are also mapped (d, e, f, respectively).



150 **4 Discussion**

151 **4.1 Distribution, mixing, and flow behaviour of the P/AG outflow**

152 Hydrographic CTD measurements in the northwestern Arabian Sea reveal spatial variability in
153 P/AG outflow characteristics. Recently, the continental shelf of the northeastern Arabian Plate
154 margin has been subdivided into two domains: a stable and an unstable shelf, based on the
155 integration of multibeam bathymetry and seismic reflection data (Abdelmaksoud et al., 2026b).
156 The outflow waters exit the Strait of Hormuz, hugging the flat continental stable shelf bathymetry,
157 with a very thin bottom-attached flow of 10-30 m (Figs. 2 and 3). This flow has high salinity,
158 temperature, and density, resulting in negative buoyancy and a compact, coherent core with high
159 P/AG_{wf} and comparatively little dilution. The flow has a sharp upper interface (high N^2),
160 indicating stable stratification (Fig. 2d). Outflows exiting dense marginal-seas typically begin as
161 thin bottom-attached plumes before being transformed by entrainment (e.g., Bower et al., 2000).
162 At the transition from the stable to the unstable shelf, the abrupt bathymetric shift serves as the
163 initial trigger for flow transformation. This transition marks an abrupt increase in the seafloor
164 depths delimited by a major gravitational collapse, i.e., northern extension of the Batinah Offshore
165 Normal Fault. The outflow suffers from rapid **geometric/hydraulic adjustment**, increasing in
166 thickness from ~20 m to ~170 m, with localized patches of $N^2 < 0$ occurring in the immediate
167 vicinity of the bathymetric transition/step (Figs. 2d and 3f). This situation is consistent with locally
168 statically unstable stratification and transient density overturning during hydraulic adjustment of
169 the bottom-attached plume across the bathymetric step (Alford et al., 2013; Jalali et al., 2017). This
170 indicates the bathymetric step is dynamically active and likely promotes enhanced turbulent
171 entrainment/mixing at the onset of plume transformation.

172

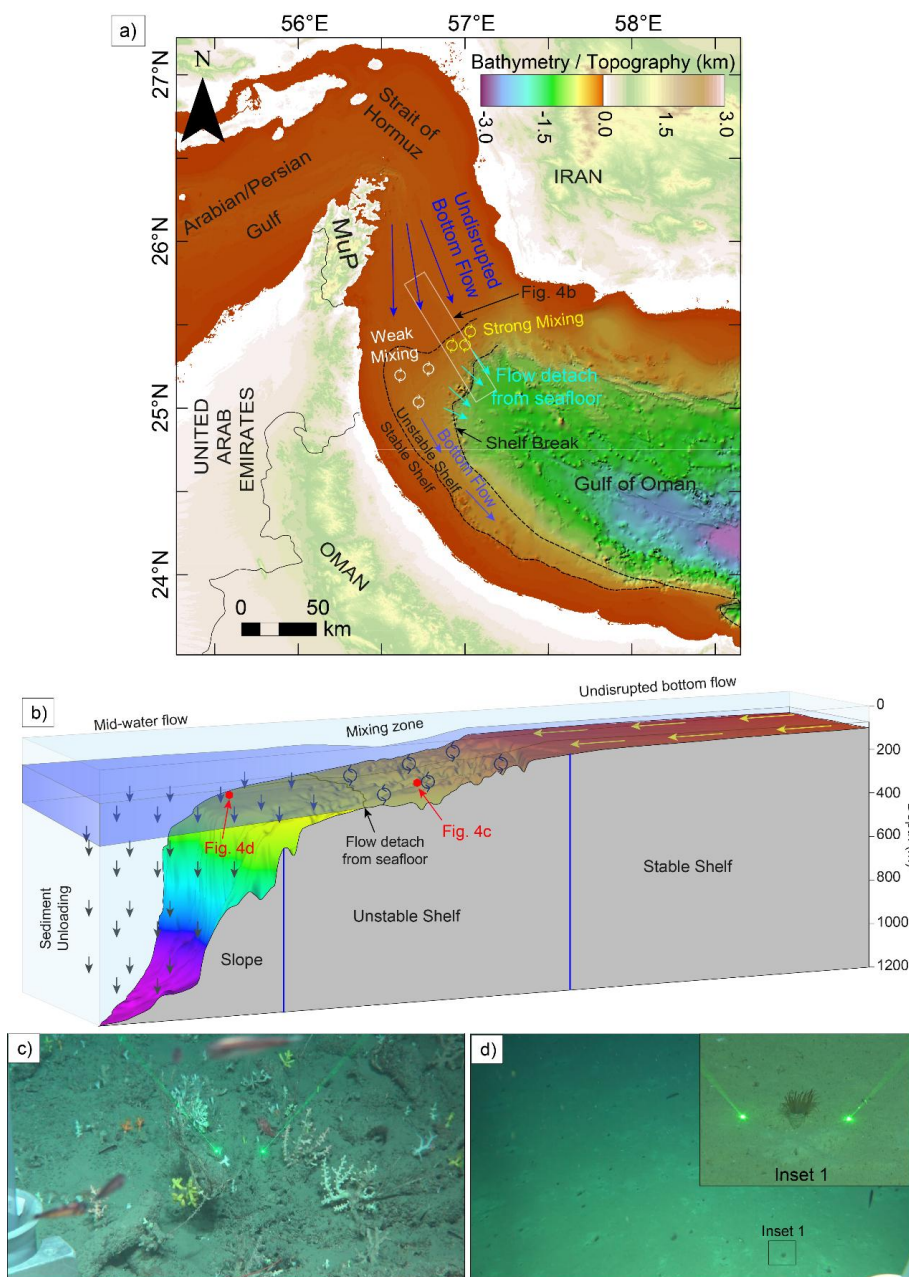


Figure 4: Map and 3D illustration of the outflow behaviour, as well as comparison of benthic communities from the bottom-attached and -detached flow. a) A map illustration of the outflow behaviour of the P/AG outflow relative to the bathymetry. b) A 3D illustration of the P/AG outflow behaviour over the stable shelf, unstable shelf, and upper slope. c and d are photos from ROV dives from the mixing zone and another representing an area where the outflow detached from the seafloor, respectively.



173 The unstable shelf has extensive crescent-shaped and elongated pockmarks and irregularities on
174 the seafloor (Abdelmaksoud et al., 2026b; Abdelmaksoud et al., 2025b). Within this domain, the
175 outflow is characterized by lower salinity, temperature, and oxygen content than the undisrupted
176 flow above the stable shelf, with continued plume thickening and weakening of P/AG_{wf}. The
177 outflow within this domain exhibits disruption, and its compact core eventually fades. There is
178 also a significant reduction of N^2 peak as well as broadening of the interfacial (across the upper
179 plume interface) N^2 stratification, which indicates erosion and weakening of the initially sharp
180 plume to ambient interface. The ambient interface is consistent with sustained interfacial
181 entrainment/mixing, dilution of the dense core, and the development of a thicker, more diffuse
182 interfacial mixing layer. Mechanistically, the roughness effect is expressed in terms of roughness
183 height relative to plume thickness, hr/H . The roughness height relative to the plume thickness
184 increases to >1 immediately after the bathymetric step. Where the roughness elements become a
185 substantial fraction of plume thickness, they enhance form drag, wake generation, and near-bottom
186 turbulence, thereby sustaining entrainment and dilution across the pockmarked shelf sector
187 (Cenedese and Adduce, 2010; Ottolenghi et al., 2017; Özgökmen and Fischer, 2008). This situation
188 is consistent with roughness-enhanced boundary-layer turbulence and hydraulic transitions
189 documented for other marginal-sea overflows (Peters & Johns, 2005; Price, 1997).

190 Once the P/AG outflow water gains enough buoyancy, it begins to detach from the seafloor above
191 the unstable shelf and to flow at an intermediate level (Fig. 4). The detached flow from the seafloor
192 has lower salinity, temperature, and oxygen content, with the top of the outflow water moving
193 towards shallower depths (Figs. 2 and 3). The intensity of the mixing and dilution of the P/AG
194 outflow changes across the unstable shelf domain. This intensity correlates with the density of
195 seafloor irregularities, with high-mixing zones found within high-density irregularities and vice
196 versa (Fig. 4a).

197 Over the lower shelf to the upper slope, the near-bottom P/AG outflow signatures weaken strongly,
198 and the P/AG_{wf} near the seabed becomes small or disappears (Fig. 2h), indicating that the bottom
199 attachment is lost and the plume persists higher in the water column. The outflow transitions into
200 a detached intermediate-depth plume, following from the preceding thickening and dilution across
201 the unstable shelf. The plume lift-off occurs approximately where the pronounced N^2 maximum at
202 the upper plume interface disappears, consistent with erosion of the initially sharp plume to the



203 ambient density interface by entrainment and dilution until the bottom-attached gravity current can
204 no longer maintain a clear near-bottom density excess. Farther offshore, the gradual re-
205 establishment of moderate N^2 suggests formation of a new, weaker and broader interface around
206 the detached plume as it adjusts toward its intermediate intrusion/neutral-buoyancy depth (Fig.
207 2d). The detached intermediate-depth plume/intrusion exhibits continued along-slope propagation,
208 and the maps (Fig. 3) suggest that, throughout the study area, the plume remains organized as a
209 margin following, bathymetrically steered boundary plume/current, with a clear shallow-
210 side/upslope limit imposed by the shelf morphology. Along-path dilution of the intermediate-depth
211 plume within the Gulf of Oman is also evident, with the plume exhibiting P/AG_{wf} of around 0.4
212 near the mouth of the Gulf (This study, Fig. 2h), and the value is reduced to less than 0.3 to the
213 south across the Omani Margin (Font et al., 2024).

214 The outflow results in further erosion and deepening of the seafloor irregularities of the unstable
215 shelf. The outflow water then carries the erosional products and deposits its load directly after
216 detaching from the seafloor above the lower shelf and slope (Fig. 2b). Strong bottom flows over
217 rough bathymetry are known to maintain thick bottom nepheloid layers through resuspension
218 (McCave, 1986; Gardner et al., 2018). Marine nepheloid layers, particularly bottom nepheloid
219 layers on continental margins, mark loci of active suspension and redeposition driven by energetic
220 near-bed currents (Biscaye and Eitrem, 1977; Gardner et al., 2018).

221 Previous hydrographic and ADCP observations show that, after exiting the Strait of Hormuz, P/AG
222 water cascades down the continental slope and spreads along the Gulf of Oman margin (Pous et
223 al., 2004). Along the Omani coast, the outflow core occurs at a depth of 200 m with a potential
224 density range of $25.5 - 27 \text{ kg/m}^3$ (Font et al., 2024). Climatological and historical analyses indicate
225 that P/AG water typically equilibrates between approximately 200 and 350 m (Prasad et al., 2001;
226 Swift and Bower, 2003). Observations off Oman document that the P/AG outflow pathway and
227 thermohaline properties vary with the mesoscale field, which can eject boundary water offshore
228 through near-shelf dipoles and lee eddies (L'hégaret et al., 2015). High-resolution simulations and
229 process analyses demonstrate that remotely generated mesoscale eddies interact with the steep
230 slope to generate frictional boundary layers and submesoscale vortices that peel P/AG water from
231 the boundary, thereby enhancing lateral dispersion and dilution (Vic et al., 2015).



232 **4.2 Oxygen modification along the P/AG outflow path and its impact on the Arabian Sea-**

233 **OMZ**

234 P/AG outflow brings high-oxygen waters from the Arabian Gulf to the Arabian Sea-OMZ, thereby
235 ventilating the OMZ. Glider observations off Oman directly demonstrate that P/AG water supplies
236 oxygen to the OMZ at intermediate depths, quantifying its ventilation contribution along the slope
237 (Font et al., 2024). Modeling further indicates that changes in Gulf properties can modulate OMZ
238 intensity by altering the density and ventilation potential of exported P/AG water (Lachkar, 2019).

239 Downstream changes in the oxygen content and pH of the outflow water show consistent dilution
240 and oxygen loss along the continental shelf. **Layer fine structure and step-like profiles along**
241 **transects indicate active mixing above the seafloor.** These results provide a high-resolution
242 continuous mapping of P/AG outflow O₂ modification along the continental shelf, linking local
243 mixing intensity to the outflow's potential to ventilate the upper oxycline of the Arabian Sea.
244 Profiles from the Gulf of Oman frequently exhibit step-like thermohaline structure and interleaving
245 consistent with double-diffusive processes that facilitate transformation of P/AG water (Ghazi et
246 al., 2017; Azizpour et al., 2017). The spatial correspondence between P/AG outflow persistence
247 and elevated near-bottom oxygen levels suggests that the upper oxycline is effectively ventilated.
248 Where the shelf-trapped P/AG water layer is strongest and most persistent, near-bottom oxygen is
249 elevated relative to adjacent waters, indicating effective ventilation near the upper oxycline depths
250 (Font et al., 2024; Swift and Bower, 2003). Downstream maps show progressive oxygen reduction
251 along the outflow pathway basinwards, reflecting dilution and consumption (Fig. 6). As mixing
252 intensity varies across the stable-unstable shelf boundary, depending on seafloor roughness, the
253 magnitude and spatial footprint of P/AG outflow ventilation depend on local thickness, attachment
254 state, and mixing intensity.

255 **4.3 Impact of the P/AG outflow on benthic life**

256 Benthic zonation closely follows P/AG outflow attachment behaviour. Where the outflow remains
257 bottom-attached, **strong near-bed shear** limits fine-sediment accumulation, maintaining exposed or
258 semi-consolidated substrate and enhancing delivery of suspended particles and oxygenated water.
259 Such conditions favor sessile suspension feeders, including corals and other epifauna, consistent



260 with the importance of hydrodynamics and substrate availability in deep-water coral ecosystems
261 (Flach et al., 1998; Roberts et al., 2006).

262 Below the detachment depth, fine sediments dominate and the hydrographic signature weakens,
263 indicating lower-energy, lower-oxygen conditions. Cerianthid tube anemones commonly occur on
264 such soft substrates and can form distinctive assemblages observable in video surveys (Davies et
265 al., 2014; Flach, 2002). The thick nepheloid layer along the lower shelf and slope may further
266 enhance food supply by retaining suspended organic matter, acting as a reservoir redistributed by
267 mixing (Hanz et al., 2019). These patterns provide a biological imprint of boundary-layer dynamics
268 and independently support the hydrographic interpretation of outflow attachment and separation.

269 **4.4 Implications for climate sensitivity of the P/AG outflow**

270 The attachment–detachment thresholds documented here imply that the P/AG outflow’s pathway
271 is sensitive to moderate shifts in source-water density, which depends strongly on the Gulf surface
272 temperature and evaporation. Warming in the P/AG would reduce outflow density, alter lift-off
273 depths, modify downstream oxygen delivery, and potentially reorganize benthic zonation along
274 the margin, indicating a climatically sensitive mechanism. Interannual to decadal changes in
275 evaporation and heat content modulate the density contrast across the Strait of Hormuz and, by
276 extension, the strength and properties of the exported outflow (Campos et al., 2020). Numerical
277 experiments indicate that warming within the P/AG reduces outflow density and weakens
278 intermediate-depth ventilation, thereby intensifying and expanding hypoxia in the Arabian Sea
279 OMZ (Lachkar, 2019; Lachkar et al., 2022). Process-resolving simulations and regional syntheses
280 indicate that where and how the outflow leaves the boundary depends on the balance between
281 buoyancy forcing and near-slope mixing (L'hégaret et al., 2015; Vic et al., 2015), so small density
282 reductions favor earlier detachment and enhanced lateral dispersion.

283 **5 Conclusions**

284 High-resolution hydrographic mapping shows that small- to mesoscale seafloor roughness
285 primarily controls mixing, thickening, and detachment of the Persian/Arabian Gulf outflow along
286 the Oman–UAE margin. Enhanced boundary-layer turbulence over irregular bathymetry drives
287 dilution, seabed detachment, and reorganization of the intermediate-depth pathway, affecting



288 oxygen delivery and sediment transport. These observations support a bathymetry-first framework
289 in which mesoscale eddies modulate downstream export but are not required to initiate
290 detachment. Because attachment and lift-off depend strongly on source-water density, moderate
291 climatic changes in Gulf heat and evaporation may alter outflow pathways and ventilation of the
292 Arabian Sea oxygen minimum zone.

293 **Acknowledgments**

294 We thank the Environment Agency Abu Dhabi (EAD) for allowing us to use their vessel, Jaywun,
295 to acquire the used CTD and bathymetry data. We thank Dr. Moamen Ali and Omar Aldhanhani
296 (Khalifa University) as well as the EAD team and the Jaywun crew for their help in acquiring the
297 data. The R/V OceanXplorer crew (led by Mattie Rodrigue and Andrew Craig) are also thanked
298 for their appreciated efforts in collecting the ROV imagery.

299 **Financial support**

300 This work was supported by Khalifa University [grant number: 8474000756].

301 **Data availability**

302 The bathymetry and CTD profiles are archived at Zenodo repository (Abdelmaksoud et al., 2025a;
303 Abdelmaksoud et al., 2026a). The regional bathymetry and topography dataset is publicly available
304 (GEBCO Compilation Group, 2025).

305 **Code availability**

306 The used TEOS-10 GSW MATLAB toolbox is publicly available (Mcdougall and Barker, 2011).
307 The Ocean Data Viewer (ODV; Schlitzer, 2024) is publicly available.

308 **Author contributions**

309 AA, AHA, and MYA conceptualized the study. AA performed data curation and formal analysis,
310 and wrote the manuscript draft. AHA, MYA, GB, and KS-M reviewed and edited the manuscript.



311 **Competing interests**

312 The authors declare there are no conflicts of interest for this manuscript.

313 **References**

- 314 Abdelmaksoud, A., Al-Suwaidi, A., and Ali, M.: CTD profiles at the mouth of the Gulf of Oman (acquired July
315 2025), *Zenodo* [dataset], <https://doi.org/10.5281/zenodo.19200743>, 2026a.
- 316 Abdelmaksoud, A., Ali, M., and Al-Suwaidi, A.: Formation Mechanism of Seafloor Gas Seeps and Pockmarks at
317 Active Continental Margins: Insights from the Gulf of Oman, *Zenodo* [dataset],
318 <https://doi.org/10.5281/zenodo.17160219>, 2025a.
- 319 Abdelmaksoud, A., Al-Suwaidi, A., Ali, M., Aldhanhani, O., Sreenivasan, S., and Steuber, T.: Geological Controls
320 on the Distribution of Pockmarks and Gas Seeps along the Northeastern Arabian Margin, *Marine Geoscience and*
321 *Energy Resources*, In Review, 2026b.
- 322 Abdelmaksoud, A., Al-Suwaidi, A., Ali, M., Shah, A., Almehairbi, S. S., Al Ali, L. M., and Ali, M. Y.: Evidence of
323 pockmarks and seafloor gas venting in the northwestern Arabian Sea, *Communications Earth & Environment*, 6, 41,
324 2025b.
- 325 Alford, M. H., Girtton, J. B., Voet, G., Carter, G. S., Mickett, J. B., and Klymak, J. M.: Turbulent mixing and
326 hydraulic control of abyssal water in the Samoan Passage, *Geophysical Research Letters*, 40, 4668-4674, 2013.
- 327 Azizpour, J., Chegini, V., and Siadatmousavi, S. M.: Seasonal variation of the double diffusion processes at the
328 Strait of Hormuz, *Acta Oceanologica Sinica*, 36, 26-34, 2017.
- 329 Biscaye, P. E. and Eitrem, S. L.: Suspended particulate loads and transports in the nepheloid layer of the abyssal
330 Atlantic Ocean, *Marine Geology*, 23, 155-172, 1977.
- 331 Bower, A. S., Hunt, H. D., and Price, J. F.: Character and dynamics of the Red Sea and Persian Gulf outflows,
332 *Journal of geophysical research: Oceans*, 105, 6387-6414, 2000.
- 333 Brewer, P. G. and Dyrssen, D.: Chemical Oceanography of the Persian Gulf, *Progress in Oceanography*, 14, 41-55,
334 1985.
- 335 Campos, E. J. D., Gordon, A. L., Kjerfve, B., Vieira, F., and Cavalcante, G.: Freshwater budget in the Persian Gulf
336 and exchange at the Strait of Hormuz, *PLOS ONE*, 15, e0238687, 2020.
- 337 Cenedese, C. and Adduce, C.: A new parameterization for entrainment in overflows, *Journal of Physical*
338 *Oceanography*, 40, 1835-1850, 2010.
- 339 Davies, J. S., Howell, K. L., Stewart, H. A., Guinan, J., and Golding, N.: Defining biological assemblages (biotopes)
340 of conservation interest in the submarine canyons of the South West Approaches (offshore United Kingdom) for use
341 in marine habitat mapping, *Deep Sea Research Part II: Topical Studies in Oceanography*, 104, 208-229, 2014.
- 342 Davila, X., Olsen, A., Lauvset, S. K., McDonagh, E. L., Brakstad, A., and Gebbie, G.: On the origins of open ocean
343 oxygen minimum zones, *Journal of Geophysical Research: Oceans*, 128, e2023JC019677, 2023.
- 344 Ditkovsky, S., Resplandy, L., and Busecke, J.: Unique ocean circulation pathways reshape the Indian Ocean oxygen
345 minimum zone with warming, *Biogeosciences*, 20, 4711-4736, 2023.
- 346 Ezam, M., Bidokhti, A. A., and Javid, A. H.: Numerical simulations of spreading of the Persian Gulf outflow into
347 the Oman Sea, *Ocean Science*, 6, 887-900, 2010.
- 348 Flach, E.: Factors controlling soft bottom macrofauna along and across European continental margins, in: *Ocean*
349 *margin systems*, edited by: Wefer, G., Billett, D., Hebbeln, D., Jørgensen, B., Schlüter, M., and van Weering, T.,
350 Springer, Berlin, Heidelberg, 351-363, 2002.
- 351 Flach, E., Lavaleye, M., De Stigter, H., and Thomsen, L.: Feeding types of the benthic community and particle
352 transport across the slope of the NW European continental margin (Goban Spur), *Progress in Oceanography*, 42,
353 209-231, 1998.
- 354 Font, J., Swart, S., Queste, B. Y., and Heywood, K. J.: Ventilation of the Arabian Sea Oxygen Minimum Zone by
355 Persian Gulf Water, *Journal of Geophysical Research: Oceans*, 129, e2023JC020668, 2024.
- 356 Gardner, W. D., Richardson, M. J., and Mishonov, A. V.: Global assessment of benthic nepheloid layers and linkage
357 with upper ocean dynamics, *Earth and Planetary Science Letters*, 482, 126-134, 2018.
- 358 Ghazi, E., Bidokhti, A. A., Ezam, M., Azad, M. T., and Hassanzadeh, S.: Physical properties of Persian Gulf
359 outflow thermohaline intrusion in the Oman Sea, *Open Journal of Marine Science*, 7, 125-140, 2017.
- 360 Group, G. C.: GEBCO 2025 Grid [dataset], 10.5285/37c52e96-24ea-67ce-e063-7086abc05f29, 2025.



- 361 Gruber, N. and Galloway, J. N.: An Earth-system perspective of the global nitrogen cycle, *Nature*, 451, 293-296,
362 2008.
- 363 Hanz, U., Wienberg, C., Hebbeln, D., Duineveld, G., Lavaleye, M., Juva, K., Dullo, W.-C., Freiwald, A.,
364 Tamborrino, L., and Reichart, G.-J.: Environmental factors influencing benthic communities in the oxygen
365 minimum zones on the Angolan and Namibian margins, *Biogeosciences*, 16, 4337-4356, 2019.
- 366 Hood, R. R., Rixen, T., Lévy, M., Hansell, D. A., Coles, V. J., and Lachkar, Z.: Oxygen, carbon and pH variability
367 in the Indian Ocean, in: *Oceanography of the Indian Ocean*, Elsevier, 2023.
- 368 Jain, V., Shankar, D., Vinayachandran, P. N., Kankonkar, A., Chatterjee, A., Amol, P., and et al.: Evidence for the
369 existence of Persian Gulf Water and Red Sea Water in the Bay of Bengal, *Climate Dynamics*, 48, 3207-3226, 2017.
- 370 Jalali, M., Chalamalla, V. K., and Sarkar, S.: On the accuracy of overturn-based estimates of turbulent dissipation at
371 rough topography, *Journal of Physical Oceanography*, 47, 513-532, 2017.
- 372 Jenkins, A.: The impact of melting ice on ocean waters, *Journal of physical oceanography*, 29, 2370-2381, 1999.
- 373 L'Hégaret, P., Carton, X., Louazel, S., Boutin, G., Capet, X., and Marchesiello, P.: Mesoscale eddies and
374 submesoscale structures of Persian Gulf Water off the Omani coast in spring 2011, *Ocean Science*, 12, 687-701,
375 2016.
- 376 L'Hégaret, P., Carton, X., Duarte, R., Vic, C., Ciani, D., Baraille, R., and Corréard, S.: Mesoscale variability in the
377 Arabian Sea from HYCOM model results and observations: Impact on the Persian Gulf Water path, *Ocean Science*,
378 11, 667-685, 2015.
- 379 Lachkar, Z.: Strong Intensification of the Arabian Sea Oxygen Minimum Zone in Response to Arabian Gulf
380 Warming, *Geophysical Research Letters*, 46, 9152-9161, 2019.
- 381 Lachkar, Z., Vallivattathillam, P., and Lévy, M.: Recent expansion and intensification of hypoxia in the Arabian
382 Gulf and its drivers, *Frontiers in Marine Science*, 9, 891378, 2022.
- 383 Lachkar, Z., Levy, M., Hailegeorgis, D., and Vallivattathillam, P.: Differences in recent and future trends in the
384 Arabian Sea oxygen minimum zone: processes and uncertainties, *Frontiers in Marine Science*, 10, 1122043, 2023.
- 385 McCave, I.: Local and global aspects of the bottom nepheloid layers in the world ocean, *Netherlands Journal of Sea
386 Research*, 20, 167-181, 1986.
- 387 McDougall, T. J. and Barker, P. M.: Getting started with TEOS-10 and the Gibbs Seawater (GSW) oceanographic
388 toolbox, *Scor/iapso WG*, 127, 1-28, 2011.
- 389 Melet, A. V., Hallberg, R., and Marshall, D. P.: The role of ocean mixing in the climate system, in: *Ocean mixing*,
390 Elsevier, 5-34, 2022.
- 391 Ottolenghi, L., Cenedese, C., and Adduce, C.: Entrainment in a dense current flowing down a rough sloping bottom
392 in a rotating fluid, *Journal of Physical Oceanography*, 47, 485-498, 2017.
- 393 Özgökmen, T. M. and Fischer, P. F.: On the role of bottom roughness in overflows, *Ocean Modelling*, 20, 336-361,
394 2008.
- 395 Peters, H. and Johns, W.: Mixing and entrainment in the Red Sea outflow plume. Part II: Turbulence characteristics,
396 *Journal of Physical Oceanography*, 35, 1897-1916, 2005.
- 397 Pous, S., Carton, X., and Lazure, P.: Hydrology and circulation in the Strait of Hormuz and the Gulf of Oman.
398 Results from the GOGP99 experiment: Part II. Gulf of Oman, *Journal of Geophysical Research: Oceans*, 109,
399 C12038, 2004.
- 400 Prasad, T. G., Ikeda, M., and Prasanna Kumar, S.: Seasonal spreading of the Persian Gulf Water mass in the Arabian
401 Sea, *Journal of Geophysical Research: Oceans*, 106, 17059-17071, 2001.
- 402 Pratt, L. J. and Lundberg, P. A.: Hydraulics of rotating strait and sill flow, *Annual Review of Fluid Mechanics*, 23,
403 81-106, 1991.
- 404 Queste, B. Y., Vic, C., Heywood, K. J., and Piontkovski, S. A.: Physical controls on oxygen distribution and
405 denitrification potential in the north west Arabian Sea, *Geophysical Research Letters*, 45, 4143-4152, 2018.
- 406 Rixen, T., Cowie, G., Gaye, B., Goes, J., Gomes, H. R., Hood, R., and et al.: Present past and future of the OMZ in
407 the northern Indian Ocean, *Biogeosciences Discussions*, 2020.
- 408 Roberts, J. M., Wheeler, A. J., and Freiwald, A.: Reefs of the deep: the biology and geology of cold-water coral
409 ecosystems, *Science*, 312, 543-547, 2006.
- 410 Schlitzer, R.: Ocean data view <https://odv.awi.de>, 2024.
- 411 Schmidt, H., Getzlaff, J., Löptien, U., and Oschlies, A.: Causes of uncertainties in the representation of the Arabian
412 Sea oxygen minimum zone in CMIP5 models, *Ocean Science*, 17, 1303-1320, 2021.
- 413 Sheehan, P. M. F., Webber, B. G. M., Sanchez-Franks, A., Matthews, A. J., Heywood, K. J., and Vinayachandran, P.
414 N.: Injection of oxygenated Persian Gulf Water into the southern Bay of Bengal, *Geophysical Research Letters*, 47,
415 2020.



- 416 Stramma, L., Schmidtko, S., Levin, L. A., and Johnson, G. C.: Ocean oxygen minima expansions and their
417 biological impacts, *Deep-Sea Research Part I: Oceanographic Research Papers*, 57, 587-595, 2010.
418 Swift, S. A. and Bower, A. S.: Formation and circulation of dense water in the Persian/Arabian Gulf, *Journal of*
419 *Geophysical Research: Oceans*, 108, 4-1-4-21, 2003.
420 Vic, C., Rouillet, G., Capet, X., Carton, X., Molemaker, M. J., and Gula, J.: Eddy-topography interactions and the
421 fate of the Persian Gulf Outflow, *Journal of Geophysical Research: Oceans*, 120, 6700-6717, 2015.
422 Yao, F. and Johns, W. E.: A HYCOM modeling study of the Persian Gulf: 2. Formation and export of Persian Gulf
423 Water, *Journal of Geophysical Research: Oceans*, 115, C11018, 2010.
424